Lawrence Berkeley National Laboratory
Recent Work

Title

SURFACE AND THIN-FILM PHOTOEMISSION SPECTRUM OF NICKEL METAL: A MANY-BODY SOLUTION TO A TWO-DIMENSIONALLY PERIODIC CLUSTER

Permalink

https://escholarship.org/uc/item/2mf9n2vt

Authors

Chen, C.
Falicov, L.M

Publication Date

1989-03-01

eScholarship.org Powered by the California Digital Library
University of California

LBL-26910
Preprint

Lawrence Berkeley Laboratory
UNIVERSITY OF CALIFORNIA

Materials & Chemical Sciences Division

RECEIVED
LAWRENCE
BERKELEY LABORATORY
JUL 3 1989
LIBRARY AND
DOCUMENTS SECTION

Submitted to Physical Review B

Surface and Thin-Film Photoemission Spectrum of Nickel Metal: a Many-Body Solution to a Two-Dimensionally Periodic Cluster

C. Chen and L.M. Falicov

March 1989

TWO-WEEK LOAN COPY
This is a Library Circulating Copy
which may be borrowed for two weeks.

Prepared for the U.S. Department of Energy under Contract Number DE-AC03-76SF00098.

LBL-26910
c.2

DISCLAIMER

This document was prepared as an account of work sponsored by the United States Government. While this document is believed to contain correct information, neither the United States Government nor any agency thereof, nor the Regents of the University of California, nor any of their employees, makes any warranty, express or implied, or assumes any legal responsibility for the accuracy, completeness, or usefulness of any information, apparatus, product, or process disclosed, or represents that its use would not infringe privately owned rights. Reference herein to any specific commercial product, process, or service by its trade name, trademark, manufacturer, or otherwise, does not necessarily constitute or imply its endorsement, recommendation, or favoring by the United States Government or any agency thereof, or the Regents of the University of California. The views and opinions of authors expressed herein do not necessarily state or reflect those of the United States Government or any agency thereof or the Regents of the University of California.

LBL-26910

SURFACE AND THIN-FILM PHOTOEMISSION SPECTRUM OF NICKEL METAL: A MANY-BODY SOLUTION TO A TWO-DIMENSIONALLY PERIODIC CLUSTER*

Changfeng Chen and L. M. Falicov

Department of Physics,
University of California, Berkeley, CA 94720

and

Materials and Chemical Sciences Division,
Lawrence Berkeley Laboratory, Berkeley, CA 94720

March 1989

---

*This work was supported in part by the Director, Office of Energy Research, Office of Basic Energy Sciences, Materials Sciences Division of the U. S. Department of Energy under Contract No. DE-AC03-76SF00098.

Surface and Thin-Film Photoemission Spectrum of Nickel Metal: A Many-Body Solution to A Two-Dimensionally Periodic Cluster

Changfeng Chen and L.M. Falicov

Department of Physics,
University of California,
Berkeley, CA 94720

and

Materials and Chemical Sciences Division,
Lawrence Berkeley Laboratory,
Berkeley, CA 94720

ABSTRACT

An exact solution of a four-site crystal model with periodic boundary conditions, a {001} thin-film with face-centered-cubic crystal structure, is presented for the nickel density of electron states, as would be measured in surface-sensitive valence-band photoemission. The object is to study modifications of the many-body electronic structure in the presence of surfaces. The model consists of: (a) five d orbitals per site per spin, with nearest-neighbor hopping; (b) a one-electron occupation energy for each orbital; and (c) Coulomb repulsions between electrons on the same site. A realistic local-density-approximation one-electron structure and intrasite electron-electron interactions most generally allowed by atomic symmetry are used. Crystal-field effects and single-particle electronic structure in the nickel-film structure are discussed. The photoemission spectrum is calculated and compared with bulk results. Physical conclusions for the true nickel surface many-body states are drawn.

March 10, 1989

PACS numbers 1989 79.60.Cn, 75.30.Pd, 75.70.Ak

Surface and Thin-Film Photoemission Spectrum of Nickel Metal: A Many-Body Solution to A Two-Dimensionally Periodic Cluster

Changfeng Chen and L.M. Falicov

Department of Physics,
University of California,
Berkeley, CA 94720

and

Materials and Chemical Sciences Division,
Lawrence Berkeley Laboratory,
Berkeley, CA 94720

I. INTRODUCTION

The electronic structure of many transition metals, e.g. Fe, Co, and Ni, presents the theoretical challenge of an almost intractable, full many-body problem. These metals have a very narrow one-electron d-band width, which is of comparable magnitude with the intra-atomic Coulomb interaction. As a consequence, both band-structure effects and the Coulomb interaction must be properly taken into account in any calculation. However, it is practically impossible to find the solution of the full many-body problem in a macroscopic crystal, because of the large number of particles therein. The traditional way of dealing with this problem takes the one-particle picture as the basis and includes many-body effects only in the form of a suitably averaged single-particle exchange-correlation potential. This approach has been successful in explaining properties of both bulk crystals[1–6] and clusters[7,8]. There are however many-body effects that cannot be taken into account by this sort of averaging. An example is the valence-band photoemission satellite[9], approximately 6 eV below the Fermi level, in face-centered cubic (fcc) Ni. Much theoretical attention[10] has been focused on this feature, as well as other many-body corrections to the Ni density of emitted states. One successful treatment by Victora and Falicov[11] uses a periodic small-cluster

method[12].

The periodic small-cluster method is a full many-body approach. It treats the band-structure effects and electron-electron interaction on an equal footing. It has been successfully applied to various problems[13–25] where local many-body effects are important. In this approach, a model Hamiltonian which explicitly includes band-structure effects and many-body interactions is solved exactly. The problem is made tractable by modeling the solid as a limited-size crystal with periodic boundary conditions. This is equivalent to solving exactly a many-body problem with integrals in $\vec{k}$ space restricted to a limited sampling. It has proved to be very good at determining spatially uniform and short-range properties, but fails at any property with non-uniform long-range characteristics. Because of the limited size of the cluster, one would not expect to get a sharp phase transition in this approach, but indications of possible mechanisms involved in long-range correlations can also be obtained. The computational overhead is drastically reduced by the full use of group-theoretical techniques.

In this paper, the periodic small-cluster method is applied to study the photoemission spectrum of a two-layer *Ni*-film system. The purpose is to modify the approach of Reference 11 so as to study the surface electronic structure of *Ni* metal. Some interesting results induced by the surface are found. Surface-sensitive photoemission experiments, either integrated or resolved in energy, angle and/or spin, are suggested to test these results. The rest of this paper is organized as follows. Section II is a detailed description of the model Hamiltonian used to study the thin-film structure of *Ni* metal. Crystal-field effects in the two-layer *Ni*-film structure are discussed. Section III describes the method of calculation. Section IV presents the single-particle electronic structure of the *Ni*-film system. Insight into the problem of surface effects on the electronic structure of *Ni* metal is obtained. Section V shows the one-particle density of states that would be measured in surface-sensitive valence-band photoemission experiments. Integrated results as well as those energy-, angle- and spin-resolved

are obtained and discussed. Conclusions are given in section VI.

II. THE HAMILTONIAN

The Hamiltonian for bulk *Ni* metal is described in Reference 11. Here the same four-atom tetrahedral cluster, the smallest nontrivial *fcc* crystal, is chosen, but with periodic boundary conditions applied only in a two-dimensional plane to form a two-layer *Ni* film with (001) orientation (see Figure 1). The z axis is perpendicular to the film. This is equivalent to a restricted sampling of two points in the surface Brillouin zone. In this structure, each atom has only eight nearest neighbors instead of twelve as in bulk *fcc* crystal, i.e. four in the same layer and four in the adjacent layer. There are five *d* orbitals per atom per spin; in the presence of a cubic field, as in bulk *Ni* metal, these orbitals split into a triplet t_{2g} and a doublet e_g. In the two-layer *fcc* structure discussed here the environment for each atom is radically different from that in a bulk *fcc* crystal. The *d* orbitals further split into more energy levels. This crystal-field effect is one of the major features of the results obtained here.

The model Hamiltonian contains both single-particle and two-particle terms:

$$H = \sum_{\substack{i,j;\mu,\nu;\sigma \\ i \neq j}} t_{i\mu,j\nu}\, c^{\dagger}_{i\mu\sigma}\, c_{j\nu\sigma}$$

$$+ \sum_{i;\mu;\sigma} E_{\mu}\, c^{\dagger}_{i\mu\sigma}\, c_{i\mu\sigma}$$

$$+ \sum_{i;\mu,\nu,\lambda,\phi;\sigma,\sigma'} V_{\mu\nu\lambda\phi}\, c^{\dagger}_{i\mu\sigma}\, c^{\dagger}_{i\nu\sigma'}\, c_{i\lambda\sigma'}\, c_{i\phi\sigma} \quad . \tag{2.1}$$

Here i, j (=0,1,2,3) label atoms in the cluster; μ, ν, λ, ϕ (=1,2,3,4,5) label the five d orbitals; σ, σ' are spin labels. The single-particle hopping terms $t_{i\mu, j\nu}$ are parametrized according to the Slater-Koster scheme[26]. Note that the four-atom cluster allows for only nearest-neighbor hopping; in the restricted crystal the second-nearest neighbor of an atom is identical to itself. The intra-atomic Coulomb interactions $V_{\mu\nu\lambda\phi}$ most generally allowed by atomic symmetry[27] are used. They include a direct Coulomb integral U, an average exchange integral

$$J = \frac{1}{2}[J(e_g, e_g) + J(t_{2g}, t_{2g})],$$

and an exchange anisotropy

$$\Delta J = [J(e_g, e_g) - J(t_{2g}, t_{2g})].$$

Following Reference 11, a value of U is chosen to be 4.3 eV and the other interaction parameters are set in the ratios $U:J:\Delta J$ = 56:8:1. (The results are insensitive to the exact values of these ratios). The next largest contribution is the nearest-neighbor Coulomb term, which in the cluster makes a constant contribution and can be neglected.

A least-square fit to Wang and Callaway's result of a first-principles band-structure calculation[2] is used to determine the Slater-Koster tight-binding parameters. The results for the bulk are (with energies measured in *eV below* the Fermi level of bulk *Ni* metal): $E_{t_{2g}}$ = 1.468 eV, E_{e_g} = 2.805 eV, $(dd\sigma)$ = 0.446 eV, $(dd\pi)$ = − 0.335 eV, and $(dd\delta)$ = 0.098 eV. It is clear that the crystal-field effect is, in the dilayer, quite different from that of the bulk, because the atoms in these "surface" layers have fewer neighbors. A straightforward calculation shows that, in the case of bulk *Ni* metal, the energy shift of the doublet e_g and the triplet t_{2g} caused by crystal-field effects can be expressed as

$$\Delta E_{e_g} = -(6/5)d_{1n} + (12/5)d_{2n}, \qquad (2.2a)$$

$$\Delta E_{t_{2g}} = (4/5)d_{1n} - (8/5)d_{2n}, \tag{2.2b}$$

where

$$2\Delta E_{e_g} + 3\Delta E_{t_{2g}} = 0, \tag{2.3}$$

and d_{1n} and d_{2n} are the contributions to the energy shift from each of the first and second neighbors, which must be determined before the crystal-field splitting in the two-layer *Ni*-film structure can be calculated. From the above data one immediately obtains

$$\Delta E_{e_g} - \Delta E_{t_{2g}} = E_{e_g} - E_{t_{2g}} = 1.337\ eV. \tag{2.4}$$

To determine d_{1n} and d_{2n}, one more condition is necessary. It is assumed that

$$d_{2n}/d_{1n} = (dd\sigma)_2/(dd\sigma)_1. \tag{2.5}$$

Although this assumption is not rigorous, it is physically quite reasonable. The values of $(dd\sigma)_2$ and $(dd\sigma)_1$ are taken from Papaconstantopoulos' fit[28] to band-structure calculations. It gives $(dd\sigma)_2/(dd\sigma)_1 = 0.189$. Thereby one can easily get, from bulk data analysis, $d_{1n} = -1.075\ eV$ and $d_{2n} = -0.203$ eV.

By applying the same crystal-field effect analysis, the energy shifts in the case of the two-layer *Ni*-film structure are obtained,

$$\Delta E_{\alpha} = -(7/15)d_{1n} + (4/15)d_{2n}, \tag{2.6a}$$

$$\Delta E_{\beta} = -(17/15)d_{1n} + (44/15)d_{2n}, \tag{2.6b}$$

$$\Delta E_{\gamma} = (28/15)d_{1n} - (16/15)d_{2n}, \tag{2.6c}$$

$$\Delta E_{\delta} = \Delta E_{\varepsilon} = -(2/15)d_{1n} - (16/15)d_{2n}, \tag{2.6d}$$

where the subscripts α, β, γ, δ, and ε refer to the five d orbitals of symmetries $(r^2 - 3z^2)$, $(x^2 - y^2)$, xy, yz, and zx respectively. The position of the d levels of the *Ni*-film structure can be easily obtained. All the parameters in the Hamiltonian (2.1) for the film are summarized in Table I. It is quite surprising that crystal-field effect in

this two-layer *fcc Ni*-film structure has such a strong influence on the one-particle energies of the *d* orbitals. It can be seen that one level of *xy* symmetry, splits off the original t_{2g} triplet, rises all the way up from 1.468 *eV* to 0.213 *eV*, quite close to the Fermi level of bulk *Ni* metal. (Remember that the energies are measured *below* the Fermi level). The other two levels in the triplet, of *xz* and *yz* symmetries, drop by about 0.9 *eV*, but still stick together. The e_g doublet splits into two separate levels, with energy increases of about 0.18 *eV* and 0.35 *eV* respectively[29].

Since both theoretical[30] and experimental[31] estimates show that metallic *Ni* has 0.56 *d* hole per atom and the method used here allows only an integral number of particles in the cluster, the configuration chosen is two *d* holes in the neutral state of the 40-orbital cluster. In this configuration, there is an average of 0.5 *d* hole per atom, which is very close to the estimates mentioned above. The s-like conduction band of *Ni* metal can be treated as an electron reservoir which has "absorbed" two electrons and is not explicitly included in the calculation.

III. METHOD OF CALCULATION

With five *d* orbitals per atom per spin, there are forty orbitals in the four-atom cluster. Simple combinatorial arguments yield 780 states for two holes in the cluster. The photoemission process adds a third hole to the cluster, yielding 9880 final states. Clearly, the four-atom cluster model for *Ni* has a very large manifold of states. The symmetries inherent in the Hamiltonian (2.1) must be exploited to reduce the size of the matrices to be diagonalized. In fact, there are many symmetries in the system. First, total spin in the cluster is a good quantum number. For the case of two holes in the cluster, there are 190 triplets and 210 singlets. For the case of three holes in the cluster, there are 1140 quartets and 2260 doublets. Furthermore, there is also a space-group decomposition, which is very efficient in reducing the matrix size.

The space group for the two-layer, four-atom cluster (Figure 1) is a nonsymmorphic one, of order 16. The origin of the coordinates is chosen at site 0. In addition to the identity there is one translation (from site 0 to site 3) along the plane of the layers, the $x-y$ plane, which provide 2 operations. There are two four-fold and one two-fold rotations around the z axis (C_{4z}, C_{4z}^2, C_{4z}^{-1}). With the two intralayer translations these give 3×2 = 6 additional operations. There are also eight two-fold screw axes parallel to the $x-y$ plane (their rotation part is formed by one of the four point operations C_{2x}, C_{2y}, C_{2d}, $C_{2d'}$). This nonsymmorphic space group possesses 10 irreducible representations with the following degeneracies: γ_1 (d = 1), γ_2 (d = 1), γ_3 (d = 1), γ_4 (d = 1), γ_5 (d = 2), x_1 (d = 1), x_2 (d = 1), x_3 (d = 1), x_4 (d = 1), and x_5 (d = 2). These γ and x representations, labeled by the translation-group $\vec{k}$ vectors, correspond to the following points of the two-dimensional square Brillouin zone (which extends over the region $-2\pi/a < \pm k_x \pm k_y \leq 2\pi/a$):

$$(0, 0) \text{ for } \gamma \ , \tag{3.1}$$

$$(2\pi/a, 0) \text{ for } x \ , \tag{3.2}$$

where a is the cubic lattice constant of the fcc structure. These two points constitute the finite sampling of reciprocal space inherent in the periodic-cluster approach[12]. The character table of the group[32] is given in Table II.

The two-layer structure discussed here can be obtained directly from the original bulk structure discussed in Reference 11 by symmetry reduction. There are compatibility relations between the irreducible representations of the group of the four-atom cluster fcc bulk structure and those of the two-layer structure (see Table III). With a complete set of matrices that transform according to these irreducible representations[33], it is possible to project out sets of symmetrized basis states. Since the representations cannot mix, this is equivalent to a block diagonalization of the Hamiltonian. In the case of three holes in the cluster, the largest block is (335 × 335), a considerable

reduction from the original (9880 × 9880) matrix. The various block sizes are shown in Table IV. The solutions obtained by diagonalizing these blocks are exact solutions of the full Hamiltonian for the cluster.

IV. SINGLE-PARTICLE ELECTRONIC STRUCTURE

Before solving the full many-body problem, it is instructive to look at the one-particle energy levels in the $U = J = \Delta J = 0$ non-interacting limit to determine the changes on the electronic structure caused by single-particle effects in the presence of surfaces. In the finite, two-point sampling of the four-atom periodic cluster, there are twenty spin-independent one-electron energy levels, ten at γ and ten at x. They are distributed among the ten irreducible representations. Energies are obtained in tight-binding calculation with use of the parameters given in Table I. Results are shown in Table V, together with the bulk result of Wang and Callaway[2] for comparison. It is noticeable that, compared with the bulk result, the spread in the d levels, with one exception, shrinks by 1.1 eV. At the same time a single level of x_5 symmetry splits off the other states, ending up with an energy of 2.3 eV higher than the closest level[34]. Figure 2 is a schematic plot of the one-particle energy levels in both thin-film and bulk cases. Relevant d bands are indicated schematically in the plot. In the thin-film case, all the bands stick together in pairs. All pairs, with the exception of 9-10, are shrunk as the consequence of having fewer neighbors in the surface layers. However the band pair 9-10 is quite broad. This breadth is caused by the fact that the γ-orbital, of xy symmetry, is pointed towards nearest neighbors in the plane of film; since these neighbors are not affected by the presence of the surface, this band remains essentially bulk-like.

In Table VI the band width of each d band in both structures (note that only those bands close to the Fermi level are included) are shown together with their average values; also shown is the center of gravity of each d band and the standard

deviation which measures the scattering in the location of the centers of the d bands. It can be seen that in the thin-film case the whole range from the bottom (symmetry x_5, energy = 4.28 eV *below* the bulk Fermi level) to the top (symmetry x_5, energy = 1.22 eV *above* the bulk Fermi level) of the spectrum is 5.50 eV which is broader than the corresponding bulk value 4.32 eV. However the average d-band width (1.27 eV) in the thin-film case is considerably smaller than the value (1.55 eV) in the bulk case. If the contribution from band pair 9-10, the "bulk bands", is excluded, the average d-band width in the thin-film case is only 0.99 eV, i.e. less than 2/3 of the bulk value. The standard deviation of the center of gravity of the d bands in the bulk case (1.52 eV) is somewhat smaller than the average d-band width (1.55 eV), while in the thin-film case the standard deviation (1.33 eV) is slightly larger than the average d-band width (1.27 eV), and comparable with the bulk result. This latter feature is remarkable considering that the energy spread of 18 out of the 20 d levels shown in Table V is shrunk by 1.1 eV from the bulk value. In the thin-film case, band pair 7-8, of symmetry ($r^2 - 3z^2$), is almost flat, a characteristic feature of a surface (two-dimensional) non-bonding system.

The above results clearly show that, while the usual coherent band-structure effect is still important in producing band narrowing, the essential features of the single-particle electronic structure of the *Ni*-film system studied here is dominated by crystal-field effects, as the result of the presence of the anisotropic environment at surfaces. Qualitatively speaking, if the band-energy dispersion is expressed as

$$E(k) = c_1 + c_2 f(k),$$

then the coefficient c_1 is the dominant effect in changing the single-particle electronic structure from the band structure of bulk *Ni* metal. It determines the wide distribution of centers of gravity of the d bands, and also leads to the inhomogeneous broadening of the surface bands. Although the fine details of d-band structure of a true *Ni* metal surface may be modified in more accurate calculations, the main features given here

should remain valid.

To understand the results obtained in the periodic-cluster method, a more realistic band picture is sometimes helpful and important. In the present *Ni*-film system, it is necessary to introduce the band picture to give a correct interpretation of the results. In the restricted finite-basis calculation used in this contribution, the two holes in the four-atom cluster sit on the highest *electronic* energy level of symmetry x_5. According to Hund's rule, these two holes must be in the same spin orientation, i.e. in the minority-spin state[35]. Therefore the Fermi level will be at the x_5 majority-spin level. This is actually an atomic point of view, i.e. a discrete-level picture. In fact, in a true solid energy levels form energy bands as illustrated in Figure 2. The top band in the thin-film case (band pair 9-10) can accommodate four electrons (holes) of each spin. In this case two holes in the cluster will be in the minority-spin band which is now half filled. The majority-spin bands (9-10) are fully occupied and *below* the Fermi level. The Fermi level, on the other hand, will intersect the half-filled minority-spin band. Hence electrons *at the Fermi level* will be only of the *minority* spin, opposite to what was found in the discrete-level picture. This fact means that in an angle-integrated photoemission experiment the emitted electrons with the highest kinetic energy will be of minority spin. On the other hand, the minority-spin band is only half filled. Since the x point is at the top of the band, it is not occupied by the minority-spin electrons. Thus the emitted electrons with the highest kinetic energy in an angle-resolved photoemission experiment with angle corresponding to the x point in the surface Brillouin zone should be of majority spin, as predicted in the discrete-level picture.

It is interesting to note that, as a direct consequence of the "Fermi-level lift", the states in the s-like conduction band may change their occupation, leading to a configuration $(3d)^{9.44+\delta}\ (4s)^{0.56-\delta}$ with $\delta \neq 0$ in the surface region ($\delta = 0$ corresponds to the configuration in true bulk *Ni* metal).

One should keep in mind that all the conclusions made in this section are based on the single-particle picture. Many-body correlations modify the single-particle results and also create new features uniquely related to many-body effects. Details are given in the next section.

V. PHOTOEMISSION SPECTRUM

Photoemission experiments provide a useful probe of the electronic state in many-body systems. The physical process involved is intrinsically short-range. Therefore it should be well described in the periodic small-cluster approach.

The photoemission process adds a third hole into the system. The one-electron density of (emitted) states (DOS) is calculated by adding a hole to the two-hole ground state and projecting the result onto the eigenstates of the cluster with three holes. When hole of particular spin orientation and spatial symmetry is added, one obtains spin- and angle-resolved density of states. These may be added together to obtain the total d-band photoemission DOS.

For two holes in the cluster the Hamiltonian (2.1) yields an accidentally degenerate many-body ground state of symmetries ${}^1\gamma_3$ and ${}^3\gamma_4$. When nearest-neighbor exchange is considered ${}^3\gamma_4$ has lower energy and is henceforth considered to be the ground state. It is found to contain only holes from the x_5 one-electron orbital and has zero probability of having two holes in the same site. As a consequence there is no contribution from the on-site electron-electron interaction. The photoemission spectrum is defined as

$$F_{PE}(\varepsilon;\, \mu\sigma) = \sum_k |\langle v^{(k)}|\, C_{\mu\sigma}\, |GS\rangle|^2\, \delta(\varepsilon - \varepsilon^{(k)} + \varepsilon_{GS}) \qquad (5.1)$$

where $|v^{(k)}\rangle$ is the k-th eigenstate in the three-hole manifold of the cluster, $|GS\rangle$ is the two-hole ground state, and $\varepsilon^{(k)}$ and ε_{GS} are the corresponding eigenvalues. The operator $C_{\mu\sigma}$ destroys an electron, or equivalently creates a hole in the two-hole

ground state. The subscript μ runs over the twenty d orbitals in the cluster. The quantity

$$G(\varepsilon) = \sum_{\mu\sigma} F_{PE}(\varepsilon; \mu\sigma) \tag{5.2}$$

is called the fully integrated photoemission spectrum; the quantity

$$S(\varepsilon; \sigma) = \sum_{\mu} F_{PE}(\varepsilon; \mu\sigma) \tag{5.3}$$

is called the spin-resolved photoemission spectrum.

Figure 3 shows the fully integrated photoemission spectrum $G(\varepsilon)$. Figure 4 is spin-resolved photoemission spectrum $S(\varepsilon; \sigma)$. In all figures, the sharp lines characteristic of a finite system have been artificially broadened with Gaussian peaks of 0.2-eV halfwidth. Some interesting differences from the bulk results can be seen immediately. Compared with the result of bulk *Ni* metal[11], the most pronounced feature is the drastic reduction of the intensity of the peak at and immediately below the Fermi level. Most of the intensity is shifted to energies 2 - 5 *eV* below the Fermi level. This intensity shift is essentially caused by the energy-level rearrangement resulting from the crystal-field effect in the presence of surfaces, as discussed in sections II and IV. Another important feature is related to the satellite part of the spectrum, i.e. the peak around 7 *eV* below the Fermi level. It is broader and its relative intensity is much higher, compared with the main satellite peak in the bulk case[11]. This latter feature implies that correlation effects are stronger in the thin-film structure, because of the geometric confinement in the presence of surfaces.

The ground state of the cluster contains two holes, it must also contain thirty-eight electrons. For this reason, the photoemission spectrum is quite complicated. Nevertheless, the gross features can still be understood based on the single-particle picture given in section IV, although one should keep in mind that real situation is much more complicated. In the full many-body approach configuration interaction mixes all

one-particle levels, and all satellites in the photoemission spectrum are produced by electron-electron interactions, which are not taken into account in the single-particle picture. Figure 5 shows the energy-resolved spectrum of the probability of finding two holes on the same site after photoemission. It can be seen that the three-hole eigenstates corresponding to the "main-line" spectrum [$E > E_0$; E_0 is the location of the lowest single-electron state at x in the d band according to the single-particle calculation] exhibit a greatly reduced probability of finding two holes in one atom, as opposed to 50% in a random state created from the ${}^3\gamma_4$ ground state. As a consequence, exchange splitting within the main line is small (see Figure 4), as was the case in the bulk results[11]. However, three-hole eigenstates in the satellite part of the spectrum have a very high probability of finding two holes in one atom, which leads to a sizable exchange splitting, as can be seen in Figure 4.

The "main line" contains decreased probability of two electrons being on one site; the electrons are repulsively correlated, avoid each other and produced a narrower one-electron band. This narrowing was also observed, experimentally[9] and theoretically[10], in the bulk.

From Figure 4 one can see that the peak at the Fermi level has only the majority-spin weight. Further study shows (see Figure 6) that all the weight of this peak comes from the contribution of the emitted electrons of x_5 symmetry, as expected. This peak should be observed in an surface-sensitive spin- and angle-resolved (corresponding to the x point in the surface Brillouin zone) photoemission experiment. However, as discussed in section IV, in a spin-resolved photoemission experiment one should find that the emitted electrons of the highest kinetic energy (i.e. the electrons emitted from the Fermi level) are in the minority-spin orientation, which is the result of the Stoner model applied to a more realistic band picture. [Note that in the bulk *Ni* case[11] one does not have to introduce the band picture to interpret experimental results; the top *electronic* X_5 level can accommodate six electrons (holes) and

there are only two holes sitting on that level in the neutral state of the cluster, i.e. there are still six majority-spin electrons and four minority-spin electrons; exchange interactions between the electrons with opposite spin orientations can be properly taken care of with a discrete-level approach.]

The two-hole ground state ${}^3\gamma_4$ is fully polarized. This means that the ratio of the populations of up- and down-spin states in the ground state should be 20/18 (there are two holes in the four-atom cluster, i.e. thirty-eight electrons in the cluster). Therefore the following sum rule of the relative polarization should hold,

$$(I_+ - I_-)/(I_+ + I_-) = (20-18)/(20+18) = 2/38 \approx 5.3\%. \qquad (5.4)$$

where I_+ and I_- are the total intensities of the majority- and minority-spin states. One interesting feature of the photoemission spectrum of the *Ni*-film system is that even if the total emission is only 5.3% polarized, some energy-resolved peaks are nonetheless highly polarized. Table VII shows the relative polarization of the major peaks in the photoemission spectrum. In a surface-sensitive spin- and energy-resolved photoemission experiment one should be able to observe these highly polarized peaks with the polarization direction alternating as the energy changes.

Figure 7 and Figure 8 present the angle-resolved photoemission spectrum, corresponding to the γ and x points in the surface Brillouin zone. It is worth noting that the spectra corresponding to the two points are very different.

The spectrum corresponding to the γ point has a single large peak located about 2 *eV* below the Fermi level (within the main line), while some much weaker peaks spread out in a quite broad energy range. There is no peak at or near (within 1.0 *eV* range) the Fermi level. The spin polarization of the major peak in the main line is weak (about 13%). The intensity of the peaks in the satellite part is low; however the polarizability is very high -- almost fully polarized in the majority-spin orientation.

On the other hand, the spectrum corresponding to the x point has several peaks close together in the main line. The peak at the Fermi level is fully polarized in the majority-spin orientation. The other peaks in the main line are not highly polarized (relative polarization is less than 10% in the minority-spin orientation). There is a pronounced satellite peak around 7.0 eV below the Fermi level; its relative intensity is very high and thus it should be easily observable in a surface-sensitive photoemission experiment. Comparison of Figures 6 and 8 shows that the dominant contribution to the photoemission spectrum corresponding to $\vec{k} = x$ comes from the states of x_5 symmetry.

The density of calculated emitted one-electron states presented in this section should be compared with surface-sensitive valence-band photoemission experiments with incident-photon energies in a range such that the penetration depth of the photons is about one single atomic layer. The results obtained in this contribution, which are characteristic of the electronic structure of Ni metal surface, should be observed. Although details of the real structure may be different, the main features should remain correct because of the very large contribution of the many-body effects.

VI. CONCLUSION

A many-body periodic small-cluster model of $3d$ electrons for a {001} dilayer of fcc Ni has been studied to explore the modification of the electronic structure in the presence of surfaces. This approach incorporates both band-structure effects and many-body correlations on an equal footing, and presents an exactly soluble model for such a highly correlated system. It is found that the crystal-field effect plays an important role in determining the essential features of the electronic structure in the presence of surfaces. The ground-state properties and the photoemission spectrum close to the Fermi level are dominated by the single-particle terms in the Hamiltonian, although electron-electron correlation effects produce the expected band narrowing.

The single-particle terms are strongly altered from the bulk structure by the anisotropic environment at surfaces, leading to a "Fermi-level lift" and consequently a slight change of *d* electron population in the surface region. There is a considerable reduction (from the independent-particle picture) of the probability of finding two holes in one atom, in the states close to the Fermi level of the photoemission spectrum. As a consequence, the exchange splitting in most of the spectrum is very small, and thus a single-particle picture provides a reasonably good description. Exchange splitting in the satellite part is fairly large, corresponding to a high probability of finding two holes in one atom. Compared to the bulk result, the main satellite peak in the *Ni*-film photoemission spectrum is broader and has a higher relative intensity. This result shows that correlation effects in this thin-film structure are stronger than those in the bulk *Ni* metal, because of geometric confinement introduced by the presence of surfaces and its consequent band narrowing, many-body effects are more important. Some new features characteristic of the surface electronic structure of *Ni* metal are revealed. Surface-sensitive valence-band photoemission experiments should be able to test the results reported here.

ACKNOWLEDGMENT

The authors would like to thank Dr. Ariel Reich for many stimulating discussions and his help with the computer codes at the early stages of this work. This research was supported, at the Lawrence Berkeley Laboratory, by the Director, Office of Energy Research, Office of Basic Energy Sciences, Material Sciences Division, U.S. Department of Energy, under contract No. DE-AC03-76SF00098.

REFERENCES

1 R.A. Tawil and J. Callaway, Phys. Rev. B **7** , 4242 (1973).

2 C.S. Wang and J. Callaway, Phys. Rev. B **15** , 298 (1977).

3 J. Callaway and C.S. Wang, Phys. Rev. B **16** , 2095 (1977).

4 C.S. Wang, R.E. Prange, and V. Korenman, Phys. Rev. B **25** , 5766 (1982).

5 H.S. Greenside and M.A. Schlüter, Phys. Rev. B **27** , 5 (1983).

6 K.B. Hathaway, H.J.F. Jansen, and A.J. Freeman, Phys. Rev. B **31** , 12 (1985).

7 K. Lee, J. Callaway, and S. Dhar, Phys. Rev. B **30** , 1724 (1984).

8 E.M. Haines, V. Heine, and A. Ziegler, J. Phys. F **15** , 661 (1985); **16** , 1343 (1986).

9 S. Hufner and G.K. Wertheim, Phys. Lett. **51A** , 299 (1975); C. Guillot, Y. Ballu, J. Paigne, J. Lecante, K.P. Jain, P. Thirty, R. Pinchaux, Y. Petroff, and L.M. Falicov, Phys. Rev. Lett. **39** , 1632 (1977); D.E Eastman, F.J. Himpsel, and J.A. Knapp, *ibid.* **40** , 1514 (1978); F.J. Himpsel, J.A. Knapp, and D.E Eastman, Phys. Rev. B **19** , 2919 (1979); L.A. Feldkamp and L.C. Davis, Phys. Rev. Lett. **43** , 151 (1979); W. Eberhardt and E.W Plummer, Phys. Rev. B **21** , 3245 (1980); L.A. Feldkamp and L.C. Davis, *ibid.* **22** , 3644 (1980); R. Clauberg, W. Gudat, E. Kisker, E. Kuhlmann, and G.N. Rothberg, Phys. Rev. Lett. **47** , 1314 (1981); L.C. Davis, J. Appl. Phys. **59** , 25 (1986).

10 D.R. Penn, Phys. Rev. Lett. **42** , 921 (1979); A. Liebsch, *ibid.* **43** , 1431 (1979); N. Martensson and B. Johansson, *ibid.* **45** , 482 (1980); L.C. Davis and L.A. Feldkamp, Solid State Commun. **34** , 141 (1980); A. Liebsch, Phys. Rev. B **23** , 5203 (1981); L. Kleinman and K. Mednick, *ibid.* **24** , 6880 (1981); G. Treglia, F. Ducastelle, and D. Spanjaard, J. Phys. (Paris) **43** , 34 (1982); T. Aisaka, T. Kato, and E. Haga, Phys. Rev. B **28** , 1113 (1983); R. Clauberg, *ibid.* **28** , 2561 (1983).

11 R.H. Victora and L.M. Falicov, Phys. Rev. Lett. **55** , 1140 (1985).

12 L.M. Falicov, in *Recent Progress in Many-Body Theories* , edited by E. Pajanne and R. Bishop, Volume I, (Plenum, New York, 1988), p. 275.

13 L.M. Falicov and R.H. Victora, Phys. Rev. B **30** , 1695 (1984).

14 A. Reich and L.M. Falicov, Phys. Rev. B **34** , 6752 (1986).

15 J.C. Parlebas, R.H. Victora, and L.M. Falicov, J. Phys. (Paris) **47** , 1029 (1986).

16 E.C. Sowa and L.M. Falicov, Phys. Rev. B **35** , 3765 (1987).

17 E.C. Sowa and L.M. Falicov, Phys. Rev. B **37** , 8707 (1988).

18 A. Reich and L.M. Falicov, Phys. Rev. B **36** , 3117 (1987).

19 A. Reich and L.M. Falicov, Phys. Rev. B **37** , 5560 (1988).

20 A. Reich and L.M. Falicov, Phys. Rev. B **38** , 11199 (1988).

21 C.R. Proetto and L.M. Falicov, Phys. Rev. B **38** , 1754 (1988).

22 C.F. Chen, A. Reich, and L.M. Falicov, Phys. Rev. B **38** , 12823 (1988).

23 J. Callaway, D.P. Chen and R. Tang, Z. Phys. D **3** , 91 (1986);
Phys. Rev. B **35** , 3705 (1987).

24 J. Callaway, Phys. Rev. B **35** , 8723 (1987).

25 J. Callaway, D.P. Chen, D.G. Kanhere, and P.K. Misra, Phys. Rev. B **38** , 2583 (1988).

26 J.C. Slater and G.F. Koster, Phys. Rev. **94** , 1498 (1954); corrected and extended to include higher angular momentum by R.R. Sharma, Phys. Rev. B **19** , 2813 (1979).

27 M. Tinkham, *Group Theory* and *Quantum Mechanism*, (Mcgraw-Hill, New York, 1964).

28 D.A. Papaconstantopoulos, *Handbook of the Band Structure of Elemental Solids*, (Plenum Press, New York, 1986), pp.111-118. To be self-consistent, *both*

$(dd\sigma)_1$ and $(dd\sigma)_2$ are taken from this book. Required spin-independent values are obtained by averaging up- and down-spin values.

29 The crystal-field calculations are made so as to keep the center of gravity of the d-manifold constant. The large change found for the xy orbital is in fact caused by a consistent change by the other four orbitals and a large resulting motion of the center of gravity.

30 V.L. Moruzzi, J.F. Janak, and A.R. Williams, *Calculated Electronic Properties of Metals*, (Pergamon, New York, 1978).

31 H. Dannan, R. Heer, and A.J.P. Meyer, J. Appl. Phys. **39** , 669 (1968). The measured *Ni* moment, $0.616\mu_B$, is believed to reflect a net spin imbalance of 0.56, with a g factor of 2.2.

32 L. P. Bouckaert, R. Smoluchowsky and E. Wigner, Phys. Rev. **50** , 58 (1936).

33 A.W. Luehrmann, Adv. Phys. **17** , 1 (1968).

34 There is an apparent rise in the Fermi level of 1.223 *eV* caused by the convention of zero-displacement of the center of gravity of the d-manifold.

35 Any use of the words "majority" or "minority" in the context of the spin orientation of an energy level refers to *electronic* spin, not the spin of the hole. In particular, if the spin orientations of all the holes in the ground state are the same, these holes are in minority-spin levels.

Table I.

Hamiltonian parameters (energies are in *eV below* the Fermi level of bulk *Ni* metal). The subscripts α, β, γ, δ, and ε refer to the *d* orbitals of symmetries $(r^2 - 3z^2)$, $(x^2 - y^2)$, xy, yz, and zx respectively.

$(dd\sigma)$	0.446
$(dd\pi)$	-0.335
$(dd\delta)$	0.098
e_α	2.451
e_β	2.625
e_γ	0.213
e_δ	2.363
e_ε	2.363
U	4.3
J	0.614
ΔJ	0.077

TABLE II.

The character table of the four-atom-cluster nonsymmorphic space group for the two-layer thin-film structure of Figure 1.

	1	1	1	1	2	2	2	2	2	2
	E	E	C_{4z}^2	C_{4z}^2	$C_{4z};C_{4z}^{-1}$	$C_{4z};C_{4z}^{-1}$	$C_{2x};C_{2y}$	$C_{2x};C_{2y}$	$C_{2d};C_{2d'}$	$C_{2d};C_{2d'}$
	0	3	0	3	0;3	3;0	1;2	2;1	1;2	2;1
γ_1	1	1	1	1	1	1	1	1	1	1
γ_2	1	1	1	1	1	1	-1	-1	-1	-1
γ_3	1	1	1	1	-1	-1	1	1	-1	-1
γ_4	1	1	1	1	-1	-1	-1	-1	1	1
γ_5	2	2	-2	-2	0	0	0	0	0	0
x_1	1	-1	-1	1	i	-i	1	-1	i	-i
x_2	1	-1	-1	1	-i	i	1	-1	-i	i
x_3	1	-1	-1	1	-i	i	-1	1	i	-i
x_4	1	-1	-1	1	i	-i	-1	1	-i	i
x_5	2	-2	2	-2	0	0	0	0	0	0

TABLE III.

Compatibility relations between the representations of the group for the bulk structure and those for the group of the two-layer thin-film structure. The original representations are given in Reference 19.

Original representations of the bulk structure	Reduce to the following representations of the two-layer structure
Γ_1	γ_1
Γ_2	γ_3
Γ_{12}	$\gamma_1 \oplus \gamma_3$
Γ_{15}	$\gamma_2 \oplus \gamma_5$
Γ_{25}	$\gamma_4 \oplus \gamma_5$
X_1	$\gamma_2 \oplus x_5$
X_2	$\gamma_4 \oplus x_5$
X_3	$\gamma_3 \oplus x_1 \oplus x_2$
X_4	$\gamma_1 \oplus x_1 \oplus x_2$
X_5	$\gamma_5 \oplus x_3 \oplus x_4 \oplus x_5$

TABLE IV.

Sizes of blocks of the various representations for the two-layer thin-film-structure space group.

		γ_1	γ_2	γ_3	γ_4	γ_5	x_1	x_2	x_3	x_4	x_5
$N = 2$	$S = 1$	8	13	8	13	24	12	12	12	12	26
	$S = 0$	19	14	17	12	24	12	12	12	12	26
$N = 3$	$S = 3/2$	70	70	69	69	146	73	73	73	73	139
	$S = 1/2$	167	167	168	168	330	165	165	165	165	335

Table V.

One-particle eigenvalues (energies are in *eV below* the Fermi level of bulk *Ni* metal) for two-layer *fcc Ni*-film structure, together with the bulk result. The degeneracies shown in the table are per spin.

Two-layer thin film			Bulk[a]		
Energy	Symmetry	Degeneracy	Energy	Symmetry	Degeneracy
-1.223	x_5	2	-0.01	X_5	6
1.065	γ_4	1	0.18	X_2	3
1.173	γ_4	1	0.92	Γ_{12}	2
1.396	x_5	2	2.04	Γ'_{25}	3
1.407	γ_5	2	3.81	X_3	3
1.505	γ_3	1	4.31	X_1	3
1.883	x_3, x_4	2			
2.125	γ_3	1			
2.367	γ_5	2			
2.371	γ_1	1			
3.795	x_1, x_2	2			
4.011	γ_2	1			
4.280	x_5	2			

[a] Reference 2. Required spin-independent one-electron energies are obtained by averaging up- and down-spin energies.

Table VI.

Average bandwidth and distribution of the center of gravity of the *d* bands in the thin-film and bulk *Ni* system. Energies are in *eV below* the bulk Fermi level. Figure 2 presents a schematic plot of the distribution of these bands. Only those bands close to the Fermi level are included.

Two-layer thin film			Bulk[a]		
band	bandwidth (*eV*)	center of gravity (*eV*)	band	bandwidth (*eV*)	center of gravity (*eV*)
1,2	1.91	3.74	1	2.27	3.74
3,4	1.43	3.08	2	1.77	3.11
5,6	0.62	1.85	3	1.86	0.65
7,8	0.01	1.40	4	0.93	0.22
9,10	2.40	-0.06	5	0.93	0.22
average	1.27	2.00	average	1.55	1.59
standard deviation		1.33	standard deviation		1.52

[a] Reference 2. See the footnote of Table V.

Table VII.

Relative polarization of the major peaks in the photoemission spectrum of the *Ni*-film system. I_+ and I_- are the intensities of the majority- and minority-spin states.

Peak	$\frac{I_+ - I_-}{I_+ + I_-}$ (%)
A	100
B	-50
C	-11
D	-8
E	-10
F	5
G	100

FIGURE CAPTIONS

Figure 1

The four-atom cluster in the two-layer fcc structure. With periodic boundary conditions this cluster, which forms an infinite two-layer slab, is equivalent to sampling the surface Brillouin zone at the points γ and x (see the text for details). For each site in the cluster, there are only eight nearest neighbors, instead of twelve as in the bulk fcc structure.

Figure 2

A schematic plot of the energy levels and the corresponding energy bands of d electrons in the thin-film and bulk Ni metal system. The symmetry of each level is shown. The numbers in parentheses are the degeneracies of the energy levels. The numbers indicating the bands are the band indices. Energies are in eV *below* the bulk Fermi level. Compatibility relations between the representations of the group for the bulk structure and those for the group of the two-layer thin-film structure can be found in Table III.

Figure 3

Total density of calculated emitted one-electron states. The Fermi level (E_f = 0.0 eV), is determined by surface electronic structure and raised by 1.223 eV relative to the bulk value. The location of the lowest single-electron state at x in the d band according to the single-particle calculation (see Table V) is denoted by E_0.

Figure 4

Total spin-resolved density of calculated emitted one-electron states. Solid lines correspond to the majority-spin states; dashed lines correspond to minority-spin states.

Figure 5

The energy spectrum of the probability of finding two holes on the same site in the three-hole eigenstates for the energy range corresponding to the calculated photoemission spectrum.

Figure 6

Spin-resolved density of calculated emitted one-electron states projected on the wave vector and symmetry x_5 of the emitted electron. Solid lines correspond to the majority-spin states; dashed lines correspond to minority-spin states. It can be seen, by comparison with Figure 4, that all the weight of the peak at the Fermi level comes from the contribution of the emitted electron with majority-spin orientation and x_5 symmetry.

Figure 7

Angle-resolved density of calculated emitted one-electron states, corresponding to the γ point in the surface Brillouin zone. Solid lines correspond to majority-spin states; dashed lines correspond to minority-spin states.

Figure 8

Angle-resolved density of calculated emitted one-electron states, corresponding to the x point in the surface Brillouin zone. Solid lines correspond to majority-spin states; dashed lines correspond to minority-spin states.

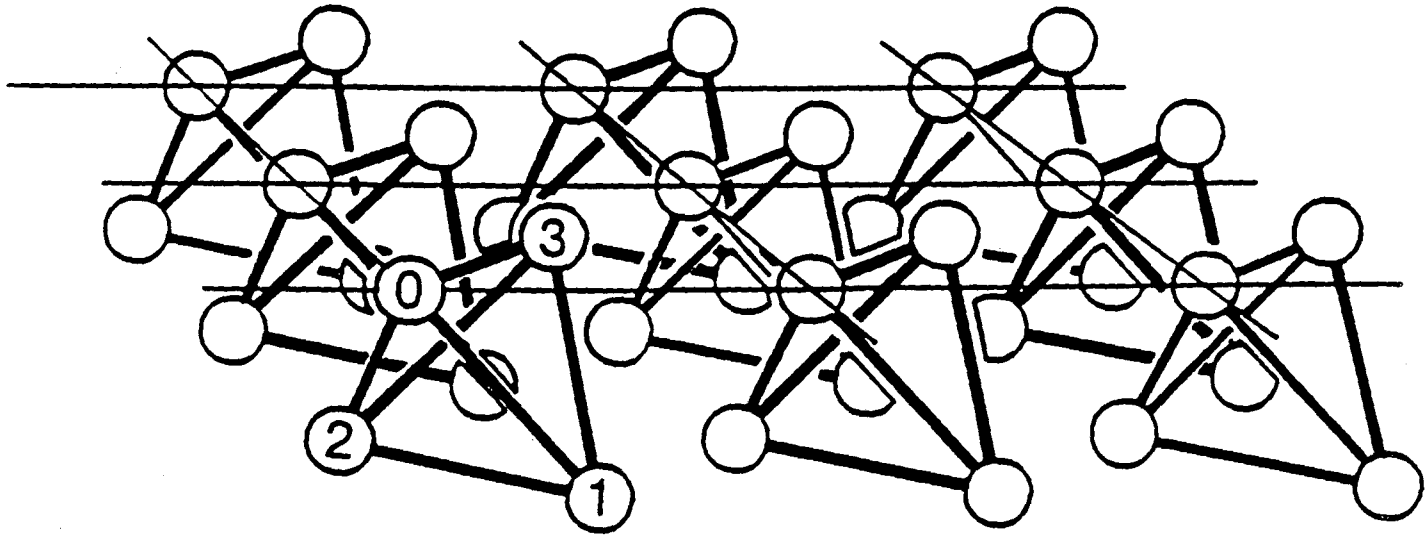

Figure 1

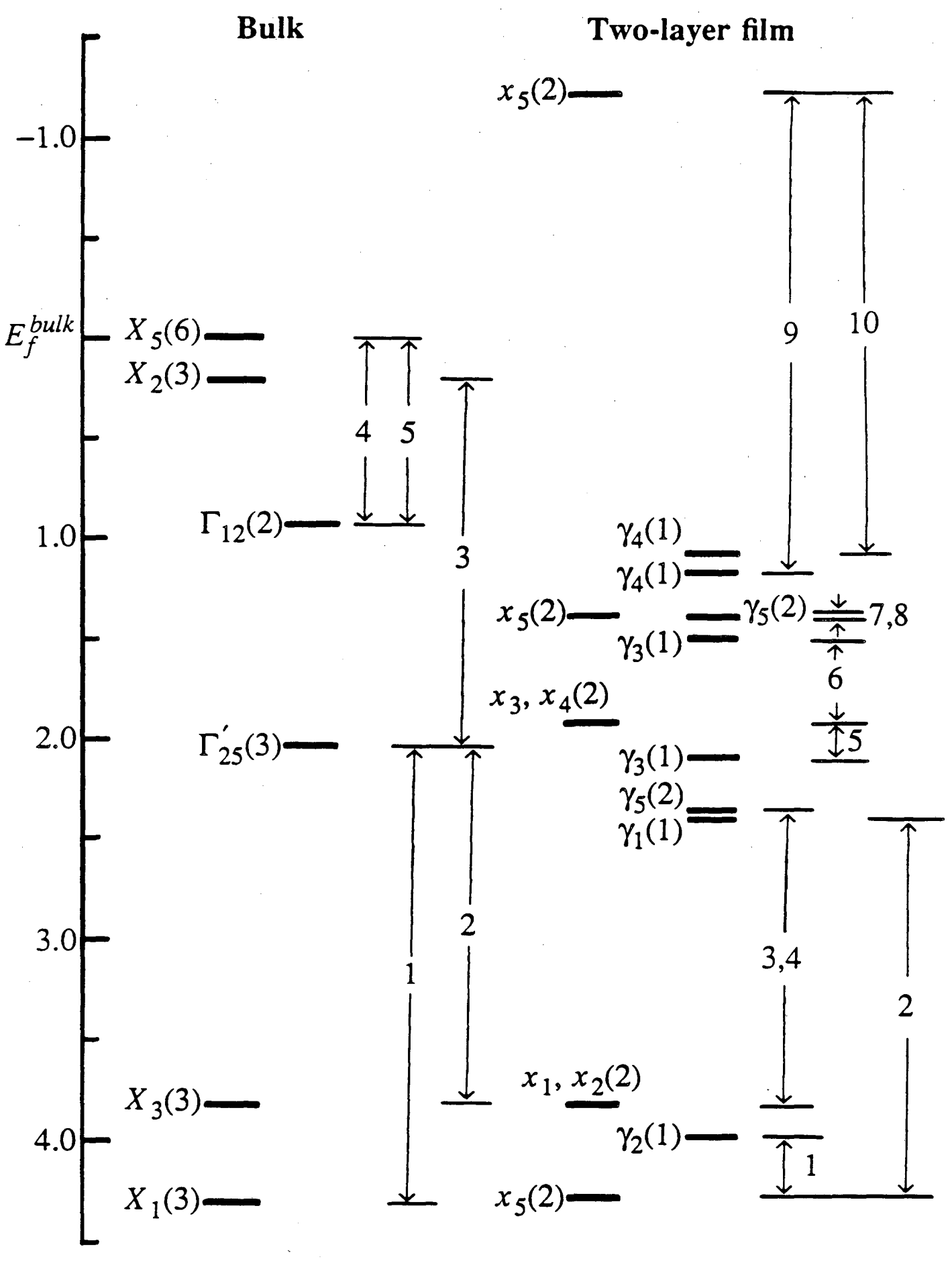
Bulk
Two-layer film
-1.0
1.0
2.0
3.0
4.0
E_f^{bulk}
$X_5(6)$
$X_2(3)$
$\Gamma_{12}(2)$
$\Gamma'_{25}(3)$
$X_3(3)$
$X_1(3)$
$x_5(2)$
$\gamma_4(1)$
$\gamma_4(1)$
$x_5(2)$
$\gamma_3(1)$
$x_3, x_4(2)$
$\gamma_3(1)$
$\gamma_5(2)$
$\gamma_1(1)$
$x_1, x_2(2)$
$\gamma_2(1)$
$x_5(2)$
$\gamma_5(2)$
7,8
9
10
6
5
4
5
3
1
2
3,4
2
1

Figure 2

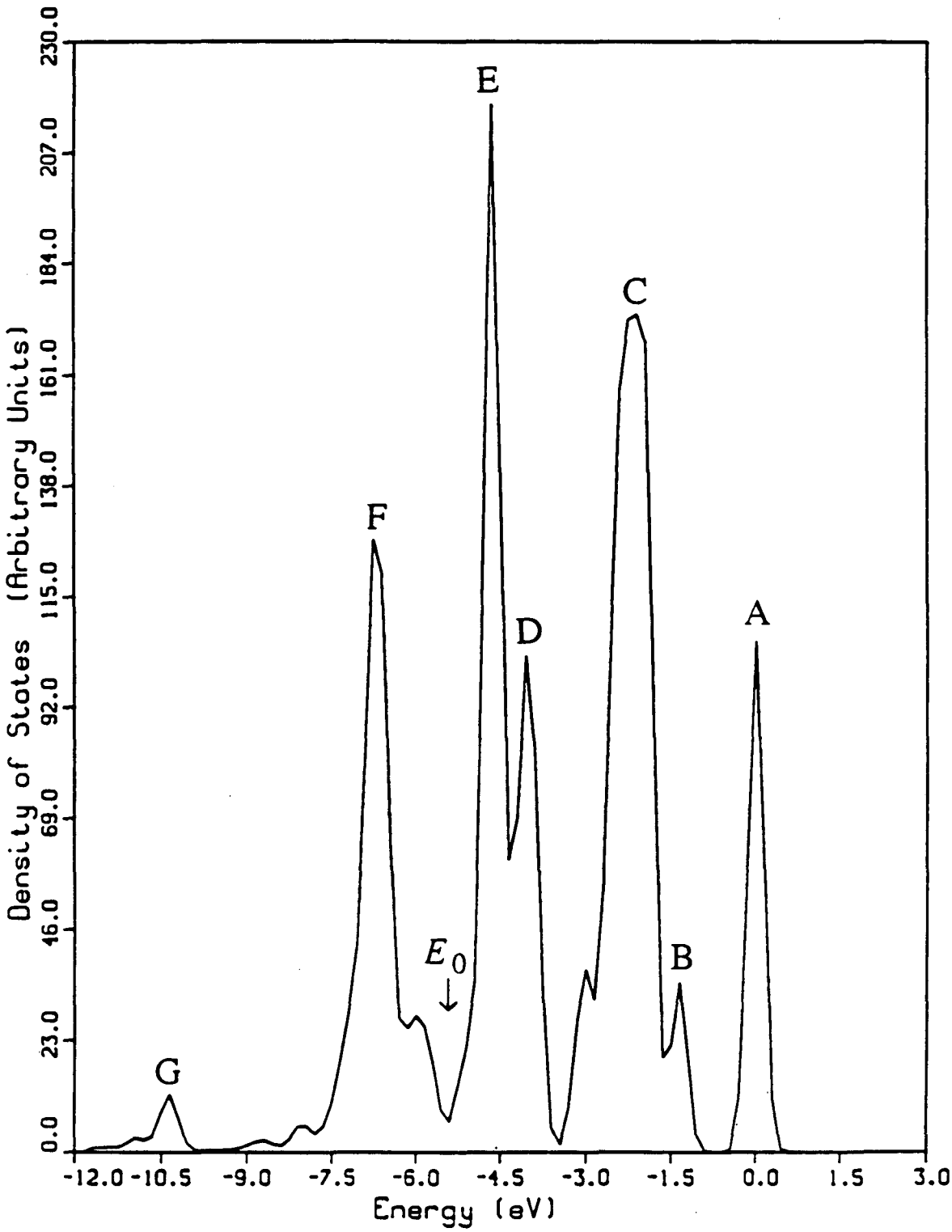
Density of States (Arbitrary Units)
0.0
23.0
46.0
69.0
92.0
115.0
138.0
161.0
184.0
207.0
230.0
-12.0
-10.5
-9.0
-7.5
-6.0
-4.5
-3.0
-1.5
0.0
1.5
3.0
Energy (eV)
G
F
E
D
C
B
A
E_0

Figure 3

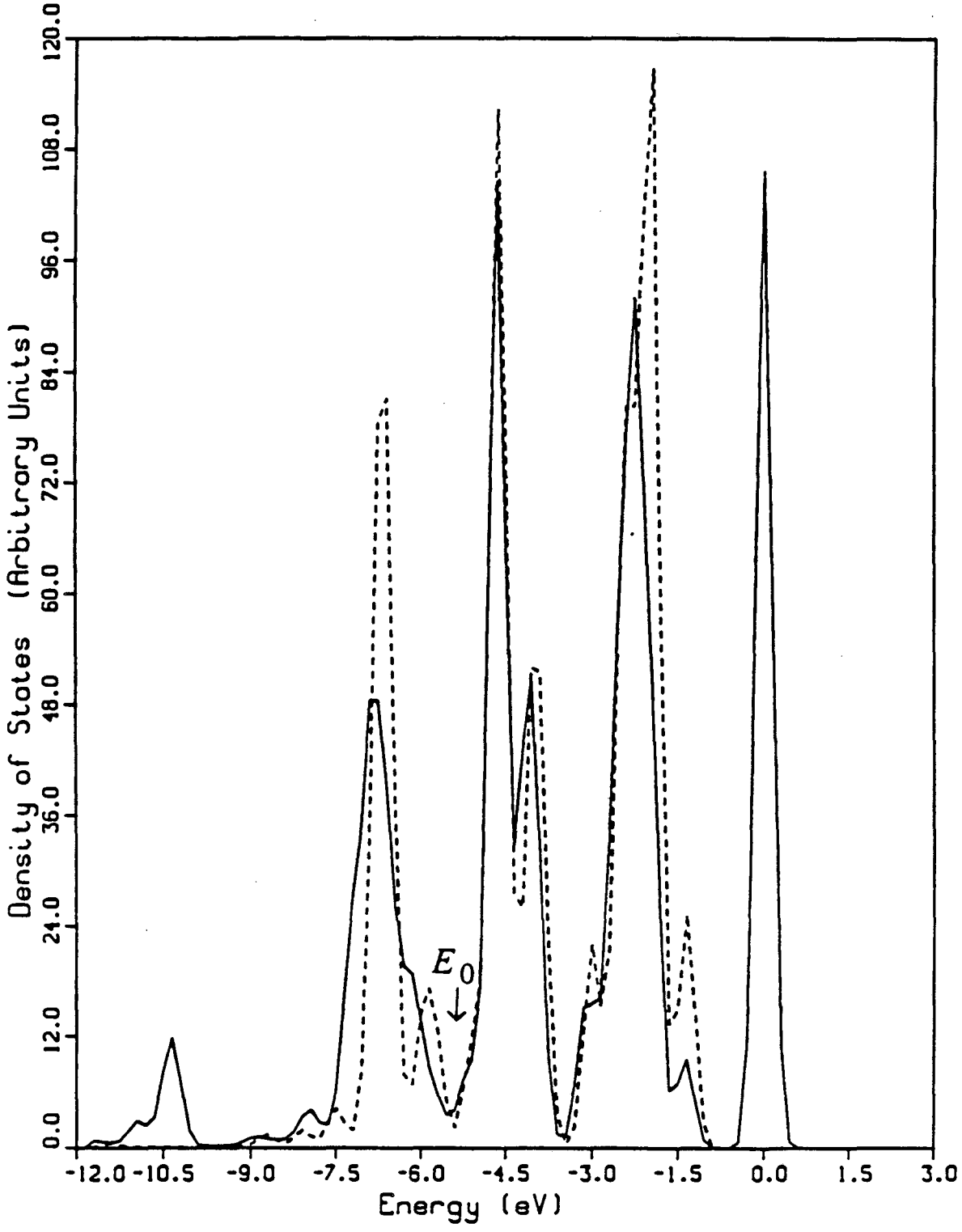
Density of States (Arbitrary Units)
0.0
12.0
24.0
36.0
48.0
60.0
72.0
84.0
96.0
108.0
120.0
E_0
-12.0
-10.5
-9.0
-7.5
-6.0
-4.5
-3.0
-1.5
0.0
1.5
3.0
Energy (eV)

Figure 4

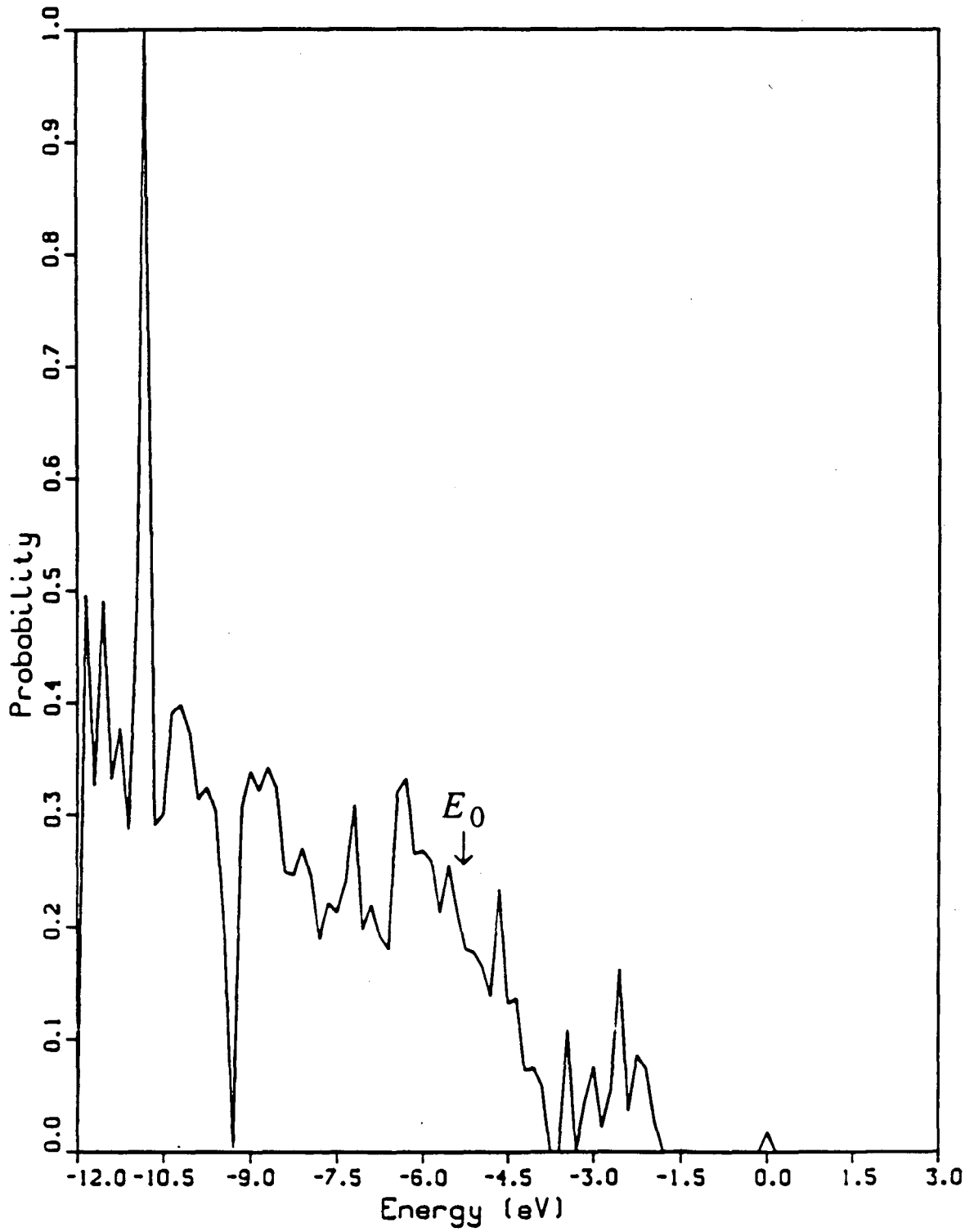
Probability
0.0
0.1
0.2
0.3
0.4
0.5
0.6
0.7
0.8
0.9
1.0
E_0
-12.0
-10.5
-9.0
-7.5
-6.0
-4.5
-3.0
-1.5
0.0
1.5
3.0
Energy (eV)

Figure 5

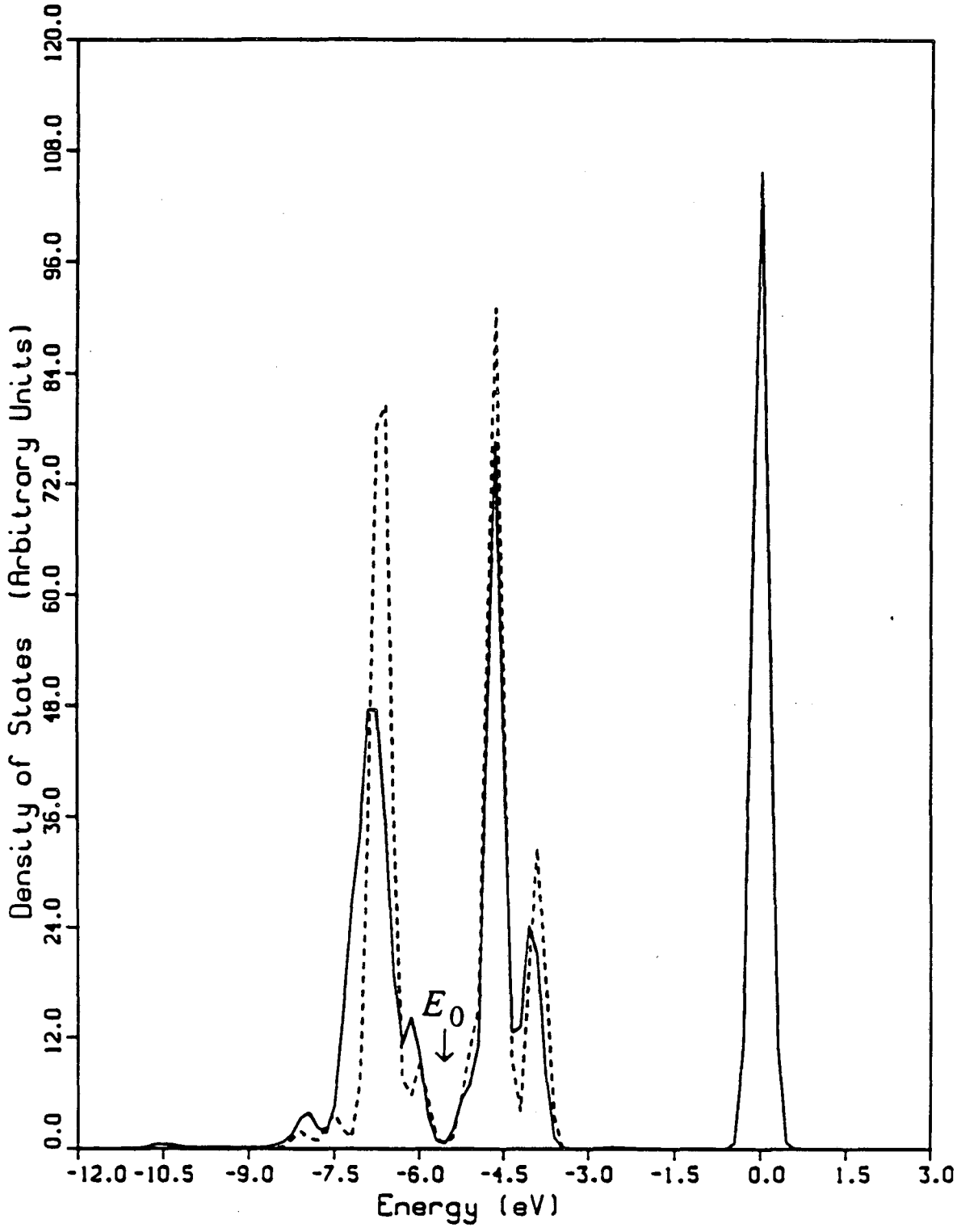
Density of States (Arbitrary Units)
0.0
12.0
24.0
36.0
48.0
60.0
72.0
84.0
96.0
108.0
120.0
-12.0
-10.5
-9.0
-7.5
-6.0
-4.5
-3.0
-1.5
0.0
1.5
3.0
Energy (eV)
E_0

Figure 6

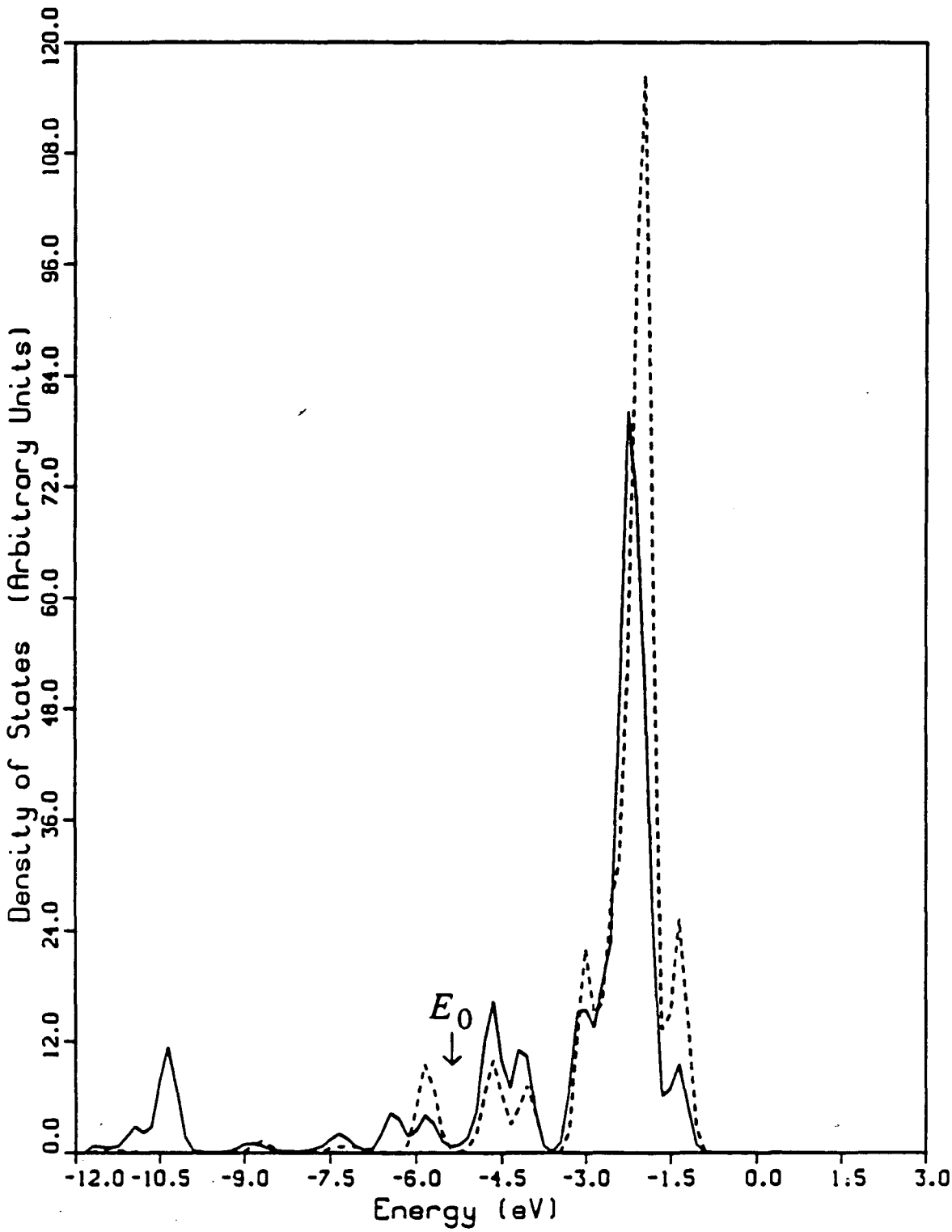
Density of States (Arbitrary Units)
0.0
12.0
24.0
36.0
48.0
60.0
72.0
84.0
96.0
108.0
120.0
E_0
-12.0
-10.5
-9.0
-7.5
-6.0
-4.5
-3.0
-1.5
0.0
1.5
3.0
Energy (eV)

Figure 7

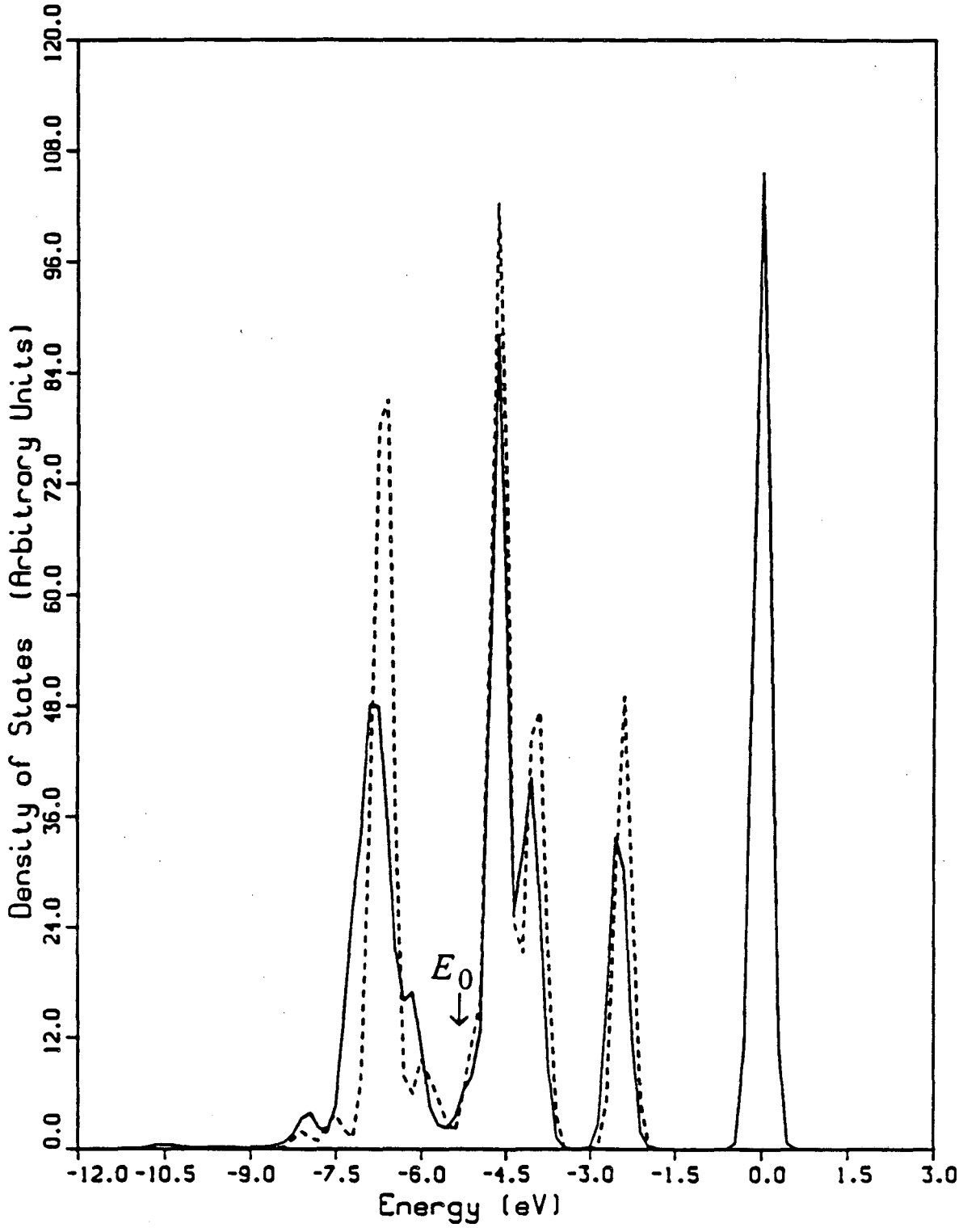
Density of States (Arbitrary Units)
0.0
12.0
24.0
36.0
48.0
60.0
72.0
84.0
96.0
108.0
120.0
-12.0
-10.5
-9.0
-7.5
-6.0
-4.5
-3.0
-1.5
0.0
1.5
3.0
Energy (eV)
E_0

Figure 8

LAWRENCE BERKELEY LABORATORY
TECHNICAL INFORMATION DEPARTMENT
1 CYCLOTRON ROAD
BERKELEY, CALIFORNIA 94720